

## Overview of HDR Large Scale PTS Thermal Mixing Experiments and Analyses with 3-D Codes and Engineering Models

L. Wolf, K. Fischer, W. Häfner

*Battelle-Institut e.V., Am Römerhof 35, D-6000 Frankfurt/Main 90, Germany*

W. Baumann, U. Schygulla, K.-H. Scholl

*Kernforschungszentrum Karlsruhe GmbH, Postfach 3640, D-7500 Karlsruhe 1, Germany*

### SUMMARY

This paper reports about experimental and analytical results of a first series of three thermal mixing experiments at HDR with high-pressure cold water injection (20°C) into one cold leg (300°C) at 11 MPa. This experimental setup leads to a localized, stripe-like asymmetric cooldown of downcomer and vessel wall. With respect to this asymmetric thermal loading, of a complete 3-D, large-scale, thick-walled PV, a first and worldwide unique data set of wall temperatures and surface strains has been generated as data and decision basis for first code validations and future fracture mechanic oriented HDR experiments. The paper summarizes the experimental results of the Preliminary Test Phase of HDR-TEMB (thermal mixing experiments) consisting of the three experiments T32.15, T32.17 and T32.18.

The experiments T32.15 ( $Fr_{CL} = 0.05$ ) and T32.18 ( $Fr_{CL} = 0.075$ ) were initiated by injecting 20°C emergency core cooling water into the stagnant cold leg filled with 300°C water at 11 MPa, whereas for experiment T32.17 ( $Fr_{CL} = 0.05$ ), the cold water was injected into the slow flowing cold leg fluid ( $Q_L/Q_{HPI} = 2$ ). For all three experiments the HP-injector closest to the vessel (1 m) which is positioned perpendicular on top of the cold leg has been used. The high system pressure of 11 MPa allows to work with extreme temperatures and thereby realistic density differences of the two fluid streams without resorting to simulating fluids. Major findings with respect to fluid mixing behavior and fluid/wall temperature cooldowns in the HPI-nozzle/cold leg region, the cold leg nozzle and along the downcomer are reported. In addition, comparisons between measured data and blind pretest predictions with the multidimensional, best-estimate codes COMMIX-1B and SOLA-PTS as well as the engineering models REMIX and VOLMIX are presented and discussed. Because these codes have been mostly validated only against experimental results obtained from small-scaled thermal mixing facilities, the HDR experiments provide an excellent opportunity to broaden the validation basis for these various computational methods.

The presentation will also summarize major highlights from the experiments of the TEMB-Main Test Phase to be performed in May/June of 1985.

## 1. INTRODUCTION

The injection of high pressure cold emergency core coolant fluid into a PWR cold leg as a result of a large or small loss-of-coolant accident in the primary system or induced by piping breaks or transient in the secondary system may lead to a severe thermal shock due to the potential of flow stratification in cold leg and downcomer because of the density difference between the cold High Pressure Injection (HPI) fluid and the hot fluid in the cold leg. The determination of the transient temperature and pressure histories in the RPV downcomer necessitates the application of complex system codes. However, none of these system codes has the ability to account for thermal stratification and thermal mixing phenomena. The resultant cold leg and downcomer temperatures are not necessarily conservative, if stratification phenomena occur. To account for these important effects much more refined and sophisticated computer codes and/or engineering calculational methods are needed. The HDR experiments expand the existing American data base for code validation.

## 2. HDR-FACILITY, PRELIMINARY TEST CONDITIONS AND OBJECTIVES

Fig. 1 shows the cross-section of the HDR-facility as used for the TEBM experiments, details of which are fully described in the design report (PHDR-Working Report No. 3.150/84, April 85). In contrast to the planar cross-section geometries tested in the American facilities with add-on plenum and standpipe core simulators, the HDR-vessel realistically possesses all vessel regions important for mixing and transfer processes. As shown in Fig. 2, three different HPI-nozzles are placed along the cold leg resembling a variety of the nozzle types in the FRG.

The Preliminary Test Series consisted of three experiments T32.15, T32.17 and T32.18 all of which were initiated at 11 MPa and 300°C fluid temperature in the cold leg and vessel. For all experiments the emergency coolant of about 20°C was injected through HPI-nozzle 1 closest to the downcomer. The three experiments were designed as follows /1/: T32.15: injection into stagnant loop,  $Fr_{CL} = 0.05$ ; T32.17: injection into slow loop flow,  $Fr_{CL} = 0.05$ ;  $Q_L/Q_{HPI} = 2$ ; T32.18: injection into stagnant loop,  $Fr_{CL} = 0.075$

The performance of these experiments at 11 MPa and the extreme difference in the fluid temperatures result in a prototypical density difference ratio,  $\Delta\rho/\rho_{sup}$  of 0.284, representative of the initial high pressure phase.

## 3. EXPERIMENTAL RESULTS

In the following, experimental, non-filtered results are shown for T32.18 and T32.17. Figs. 3 and 4 present the fluid temperature histories in the lower and upper portions of the cold leg in the vicinity of the injection jet region and close to the entrance into the downcomer together with the adjacent surface temperature at that position. Both experiments demonstrate distinct flow stratification phenomena which is in full compliance with developed flow stratification maps. Whereas for T32.18 the temperature drops by 160°C within

the first 10 min and continues to decrease, it only drops by 120°C within the first 2 min for T32.17 when it already reaches steady-state. Both experiments convincingly demonstrate that the thermal mixing processes by cold jet penetration through a hot stagnant or cross-flowing fluid are very effective. As expected, mixing is better under cross-flow conditions of cold leg fluid than under stagnant conditions. Additional thermal mixing is available between jet and downcomer to increase the temperature of the cold stratified fluid. Figs. 5 and 6 summarize the "surface temperatures" (attached to surface and shielded) at two different axial positions at the bottom cold leg together with the associated measured axial and azimuthal surface strains. The temperature histories for both experiments are nearly identical over the first minutes, thereby producing about the same maximum values for the surface strains in the order of 0.9 - 1.4 ‰. Figs. 7 and 8 present downcomer fluid temperatures at 1 and 5 cold leg diameters below the cold leg centerline as well as about half way down the downcomer. Comparing Fig. 3 with Fig. 7 clearly indicates a dramatic change of the thermal mixing processes leading to drastic fluid temperature fluctuations just below the nozzle. They demonstrate that the developing plume is unstable and characterized by penetrating hot fluid lumps towards the vessel wall leading to instantaneous temperature increases nearly up to the initial downcomer temperature. At a distance of 5  $D_{CL}$  (1 m) below the cold leg centerline, the fluid temperature close to the inside vessel wall drops only by a maximum of 50°C over 30 min for T32.18 with fluctuations changing to a more harmonic pattern of smaller amplitudes. For T32.17 with loop flow the temperature is only 10°C below the initial downcomer temperature. In both experiments additional mixing by hot fluid entrainment over a rather short distance into the cold plume is a very effective means to mitigate overcooling. Figs. 9 and 10 show the inside and outside vessel surface temperatures (gold plated inside surface grooves) together with the fluid temperatures. The inside surface temperatures are by about 30°C higher than the associated fluid temperatures for both experiments. The minimum surface temperature reaches a value of 80°C below its initial level. Finally, Figs. 11 and 12 represent measured axial and azimuthal strains at the centerline of the cold plume at the inside vessel surface. The axial strains are by about a factor of two higher than the azimuthal ones during the initial cooldown phase for both experiments. All temperature fluctuations in Figs. 9 and 10 translate into strain fluctuations with changed signs. After an initial phase, the azimuthal strains approach zero. These experimental results together with others inside and outside the plume suggest that the asymmetric cooldown stripe generates a stress field which is quite different from that calculated for recent vessel integrity studies under rotationally symmetric, global downcomer overcooling transients. Therefore, circumferential cracks may be preferentially initiated and grown under these HDR circumstances than axially oriented cracks.

#### 4. COMPARISONS BETWEEN MEASUREMENT AND BLIND PRE- AND POST-TEST PREDICTIONS

The engineering types of codes are easy to operate and inexpensive to run. They use either correlations developed on the basis of a data base (VOLMIX by Battelle based upon EPRI's transient cooldown model) or by consistently integrating the basic phenomena (REMIX by Purdue University) with the simplicity of zonal methods. Both codes need inputs and adaptations derived from previous tests and are applicable only to HPI-flows into stagnant loops. In what follows, measured data (curve 1) and the following calculations are shown: Curve 2: VOLMIX EP Battelle-Frankfurt; original EPRI entrainment correlation; Curve 3: VOLMIX 1 Battelle-Frankfurt; entrainment set equal to 1; Curve 4: REMIX BF independent Battelle-Frankfurt application; Curve 5: REMIX PUU Purdue University with updated code version.

As Figs. 13 and 14 indicate the REMIX calculations show the closest and in some positions most perfect agreement with the data in the bottom and upper parts of the cold leg. VOLMIX substantially overpredicts the cold stratified temperature at the bottom and does not correctly calculate the backflow characteristics at the top. On the other hand, as shown in Figs. 15 (1 m below cold leg centerline) and 16 (4 m below cold leg centerline) the VOLMIX EP results follow fairly closely the data, whereas REMIX PUU and BF results either overpredict or underpredict the data. Overall, the more basic approach in REMIX shows its powerful flexibility especially in the cold leg but also its limitations in the downcomer, whereas the semi-empirical approach taken in VOLMIX demonstrates its dependencies upon proper input values. However, the initial transient downcomer temperature response is simulated better than by REMIX. Finally, care must be exercised in these comparisons because local measurements are compared to zonal computational results. The best-estimate, transient, multi-dimensional codes COMMIX-1B and SOLA-PTS employ several thousand nodes, use either 2- and or 3-equations turbulence models and advanced numerical schemes to cope with the stringent requirements of jet-, stratification-, backflow- and plume modeling. Fig. 17 compares the measured data of T32.18 with SOLA-PTS predictions for the fluid temperatures at the centerline of the HPI-jet at the cold leg bottom and slightly downstream. The agreement is excellent both, in terms of initial gradients as well as temperature levels reached over the first 20 seconds. Fig. 18 compares SOLA-PTS and COMMIX-1B predictions with the measured temperature at the jet centerline position as above for experiment T32.17. Whereas SOLA-PTS used the pre-specified design values for the HPI-flow and temperature, the COMMIX-1B calculation considered the measured HPI-flow and temperature values as well as the transport delay in the HPI-line. As shown, consideration of these specific transient inflow conditions markedly improve the agreement over the first 8 seconds. Both codes demonstrate their ability to predict rather well the specific detailed characteristics of the HDR-facility without any adjustments of input parameters. This predictive capability and the additional insight into local phenomena ideally supplement the engineering codes.

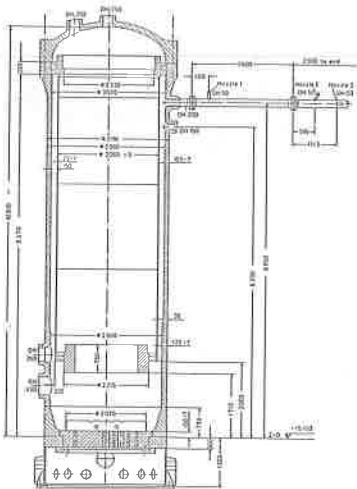


Fig. 1: Cross-Section of the HDR-Pressure Vessel

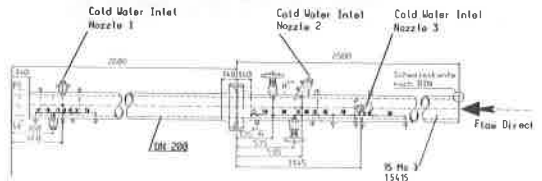


Fig. 2: Cross-Section of the HDR-Cold Leg With 3 HPI-Nozzles

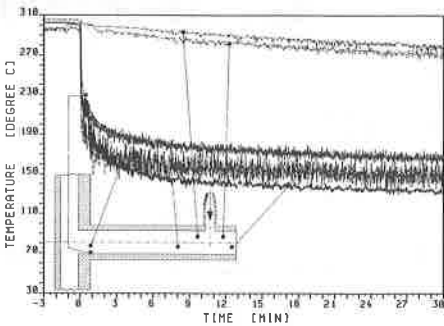


Fig. 3: T32.18: Cold Leg Fluid Temperatures

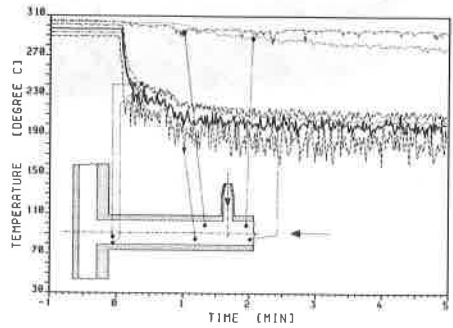


Fig. 4: T32.17: Cold Leg Fluid Temperatures

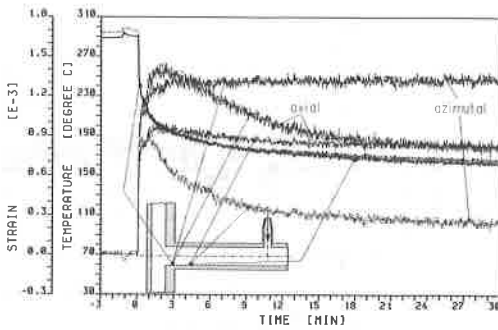


Fig. 5: T32.18: Nozzle Surface Temperatures, Axial and Azimuthal Strains

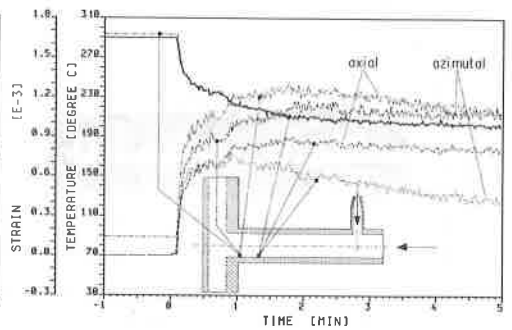


Fig. 6: T32.17: Nozzle Surface Temperatures, Axial and Azimuthal Strains

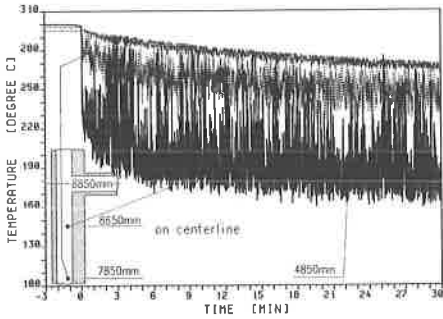


Fig. 7: T32.16: Downcomer Fluid Temperatures Near RPV Wall

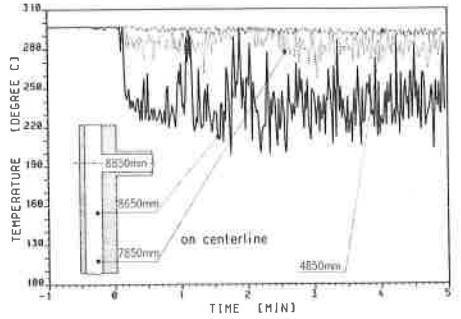


Fig. 8: T32.17: Downcomer Fluid Temperatures Near RPV Wall

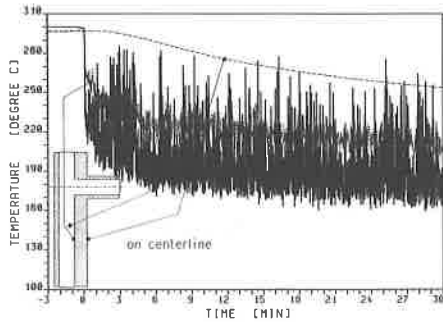


Fig. 9: T32.18: Downcomer Fluid, Inside and Outside RPV Surface Temperatures

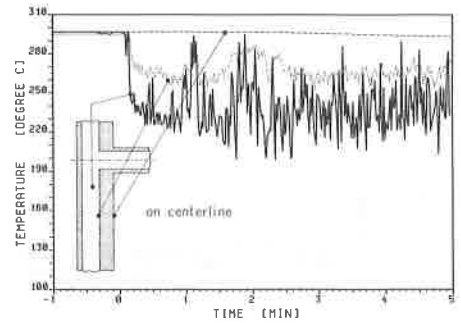


Fig. 10: T32.17: Downcomer Fluid, Inside and Outside RPV Surface Temperatures

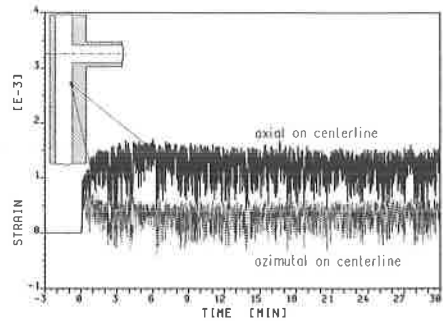


Fig. 11: T32.16: RPV-Inside Surface Strains

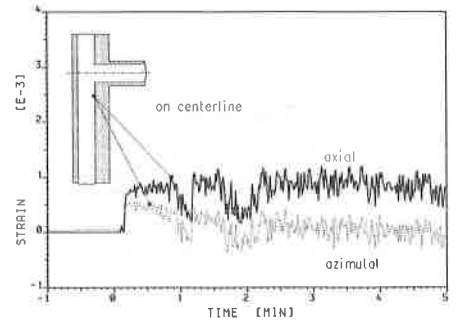


Fig. 12: T32.17: RPV-Inside Surface Strains

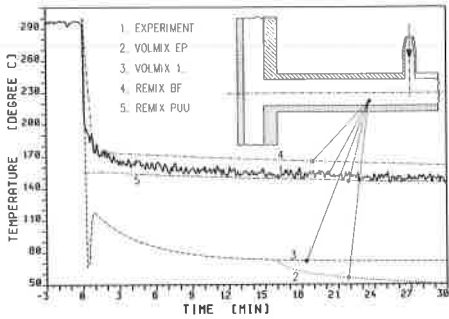


Fig. 13: T32.18: Cold Leg Bottom Temperature Comparisons With VOLMIX and REMIX Pre-Test Predictions

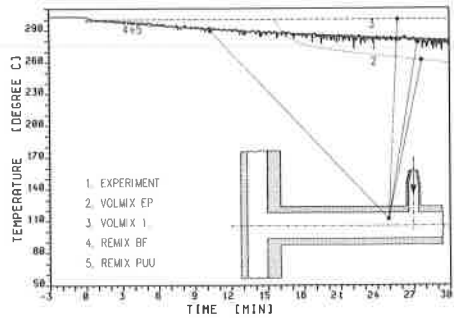


Fig. 14: T32.18: Cold Leg Top Temperature Comparisons With VOLMIX and REMIX Pre-Test Predictions

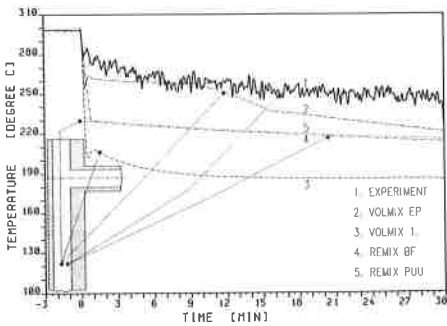


Fig. 15: T32.18: Downcomer Fluid Temperature Comparisons With VOLMIX and REMIX Pre-Test Predictions (1 m below CL)

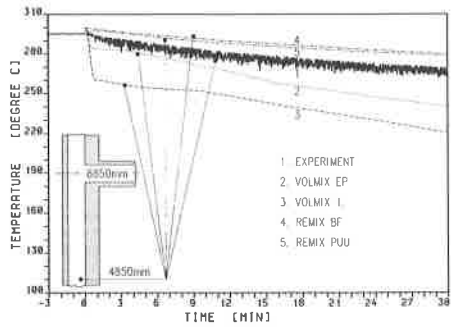


Fig. 16: T32.18: Downcomer Fluid Temperature Comparisons With VOLMIX and REMIX Pre-Test Predictions (4 m below CL)

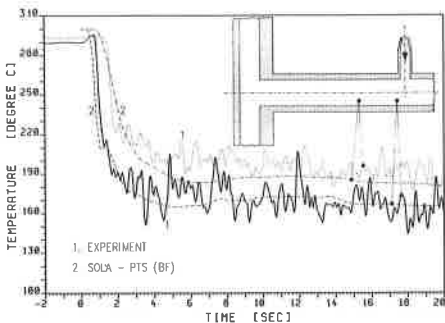


Fig. 17: T32.18: Cold Jet and Cold Leg Temperature Comparisons With SOLA-PTS Pre-Test Predictions

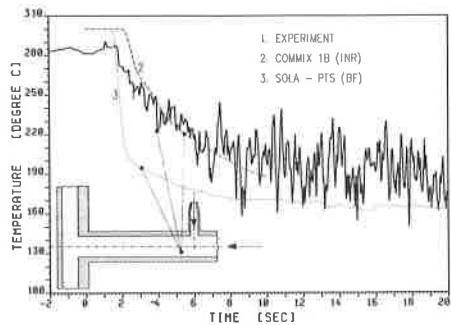


Fig. 18: T32.17: Cold Jet Temperature Comparisons With SOLA-PTS Pre- and COMMIX-18 Post Test Predictions